

See discussions, stats, and author profiles for this publication at: <https://www.researchgate.net/publication/40732465>

Dynamic Supramolecular Polymers Based on Benzene-1,3,5-tricarboxamides: The Influence of Amide Connectivity on Aggregate Stability and Amplification of Chirality

ARTICLE in CHEMISTRY - A EUROPEAN JOURNAL · DECEMBER 2009

Impact Factor: 5.73 · DOI: 10.1002/chem.200902635 · Source: PubMed

CITATIONS

35

READS

16

10 AUTHORS, INCLUDING:



Robin de Bruijn

Technische Universiteit Eindhoven

3 PUBLICATIONS 173 CITATIONS

SEE PROFILE



Evgeny A Pidko

Technische Universiteit Eindhoven

124 PUBLICATIONS 1,900 CITATIONS

SEE PROFILE



Tom F. A. de Greef

Technische Universiteit Eindhoven

60 PUBLICATIONS 2,401 CITATIONS

SEE PROFILE



Anja R A Palmans

Technische Universiteit Eindhoven

140 PUBLICATIONS 3,491 CITATIONS

SEE PROFILE

Dynamic Supramolecular Polymers Based on Benzene-1,3,5-tricarboxamides: The Influence of Amide Connectivity on Aggregate Stability and Amplification of Chirality

Patrick J. M. Stals,^[a] Jeffrey C. Everts,^[a] Robin de Bruijn,^[a] Ivo A. W. Filot,^[b]
Maarten M. J. Smulders,^[a] Rafael Martín-Rapún,^[a] Evgeny A. Pidko,^[b]
Tom F. A. de Greef,^[b] Anja R. A. Palmans,^{*,[a]} and E. W. Meijer^{*,[a, b]}



Abstract: N-Centred benzene-1,3,5-tricarboxamides (N-BTAs) composed of chiral and achiral alkyl substituents were synthesised and their solid-state behaviour and self-assembly in dilute alkane solutions were investigated. A combination of differential scanning calorimetry (DSC), polarisation optical microscopy (POM) and X-ray diffraction revealed that the chiral N-BTA derivatives with branched 3,7-dimethyloctanoyl chains were liquid crystalline and the mesophase was assigned as Col_{hc}. In contrast, N-BTA derivatives with linear tetradecanoyl or octanoyl chains lacked a mesophase and were obtained as crystalline compounds. Variable-temperature infrared spectroscopy showed the presence of threefold, intermolecular hydrogen bonding be-

tween neighbouring molecules in the mesophase of the chiral N-BTAs. In the crystalline state at room temperature a more complicated packing between the molecules was observed. Ultraviolet and circular dichroism spectroscopy on dilute solutions of N-BTAs revealed a cooperative self-assembly behaviour of the N-BTA molecules into supramolecular polymers with preferred helicity when chiral alkyl chains were present. Both the sergeants-and-soldiers as well as the majority-rules principles were operative in stacks of N-BTAs. In fact, the self-assembly of

Keywords: chirality • circular dichroism • helical compounds • self-assembly • synthesis

N-BTAs resembles closely that of their carbonyl (C=O)-centred counterparts, with the exception that aggregation is weaker and amplification of chirality is less pronounced. The differences in the self-assembly of N- and C=O-BTAs were analysed by density functional theory (DFT) calculations. These reveal a substantially lower interaction energy between the monomeric units in the supramolecular polymers of N-BTAs. The lower interaction energy is due to the higher energy penalty for rotation around the Ph–NH bond compared to the Ph–CO bond and the diminished magnitude of dipole–dipole interactions. Finally, we observed that mixed stacks are formed in dilute solution when mixing N-BTAs and C=O BTAs.

Introduction

Benzene-1,3,5-tricarboxamides (BTAs) exhibit thermotropic liquid crystalline behaviour,^[1] form organogels^[2] and lead to nanostructured materials,^[3] depending on the exact nature of the side chains employed. As a result, a variety of interesting properties and potential applications is readily at hand and fine tuning of the desired property only requires small changes in the molecular structure of this class of simple, and easily accessible organic molecules. For carbonyl (C=O)-centred BTAs, studies in the crystalline state revealed threefold intermolecular hydrogen bonds between neighbouring molecules, resulting in the formation of columnar structures.^[4] The hydrogen bonds were organised in a helical array as a result of the out of plane rotation of the amide bond with respect to the central benzene ring. In dilute alkane solutions the hydrogen bonds were retained and columnar helical supramolecular polymers with a preferred helicity were formed by introducing a chiral centre in


the alkyl side chain.^[5] A detailed study of the self-assembly process with UV and circular dichroism (CD) spectroscopy revealed a strongly cooperative mechanism in BTA self-assembly.^[5b]

While a significant amount of knowledge has become available with respect to studying and describing the self-assembly behaviour of alkyl-substituted C=O-centred BTAs, their structure–property relationship and the origin of the observed cooperativity has not received a great deal of attention. Predictive tools for the rational design of molecules that self-assemble into nano-objects of defined size, shape and stability by the molecular information stored in the chemical structure is highly important to push self-assembly one step further and to arrive at self-organisation and (catalytic) function. Therefore, we recently started a comprehensive effort to combine theoretical and experimental work to ultimately arrive at an in-depth molecular understanding of the BTA self-assembly into dynamic supramolecular polymers, a system that due to its simplicity serves as an ideal model to understand the self-assembly of more complex molecules.

We here report on the effect of a single-point mutation in the BTA design, namely changing the amide connectivity in this system, on its self-assembly behaviour. That amide connectivity in BTAs plays an important role was recently shown in the development of nucleating agents for isotactic polypropylene (*i*PP).^[6] A systematic study of nitrogen-centred (N-centred) and C=O-centred BTAs revealed that the crystallisation temperature of *i*PP was significantly increased when small amounts of BTAs were mixed in. The amide connectivity proved to play a prominent role in the nucleating and clarifying properties of the BTAs: the best performing BTA was an N-centred derivative that showed a superior

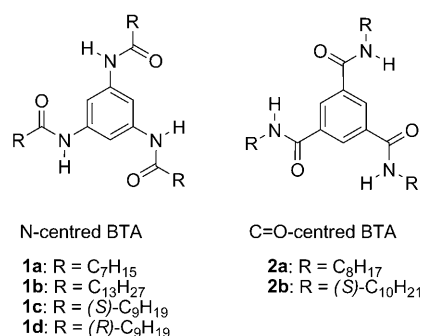
[a] P. J. M. Stals, J. C. Everts, R. de Bruijn, M. M. J. Smulders, Dr. R. Martín-Rapún, Dr. A. R. A. Palmans, Prof. Dr. E. W. Meijer
Laboratory of Macromolecular and Organic Chemistry
Eindhoven University of Technology
PO Box 513, 5600 MB Eindhoven (The Netherlands)
Fax: (+31) 402451036
E-mail: E.W.Meijer@tue.nl
a.palmans@tue.nl

[b] I. A. W. Filot, Dr. E. A. Pidko, Dr. T. F. A. de Greef,
Prof. Dr. E. W. Meijer
Institute for Complex Molecular Systems
Eindhoven University of Technology
PO Box 513, 5600 MB Eindhoven (The Netherlands)

 Supporting information for this article is available on the WWW under <http://dx.doi.org/10.1002/chem.200902635>.

clarity and almost no haze. In addition, for oligo(phenylene-vinylene)-substituted BTAs^[7] and gallic acid modified BTAs,^[8] which differed in amide connectivity, it was shown that both in solution and in the solid state N-centred derivatives were less prone to form ordered aggregates compared to C=O-centred BTAs.

Remarkably, the reasons for the significant differences in behaviour of BTA derivatives that only differ in amide connectivity have not been addressed. We anticipated that the amide connectivity in alkyl-substituted BTAs **1** and **2**, which



serve as model systems, may also have significant effects on the self assembly behaviour in dilute alkane solution with respect to the aggregate stability and the degree to which amplification of chirality takes place. We here show the synthesis and characterisation of alkyl-substituted N-centred BTAs **1a–d**. Characterisation of these new compounds in bulk was conducted with IR spectroscopy, polarisation optical microscopy (POM), differential scanning calorimetry (DSC) and X-ray diffraction. The properties of dilute alkane solutions of **1a–d** were investigated with UV/Vis and CD spectroscopy. To compare the results presented here with results previously found for C=O-centred BTAs **2a–b** (Figure 1), we include those data. The origin of the differ-

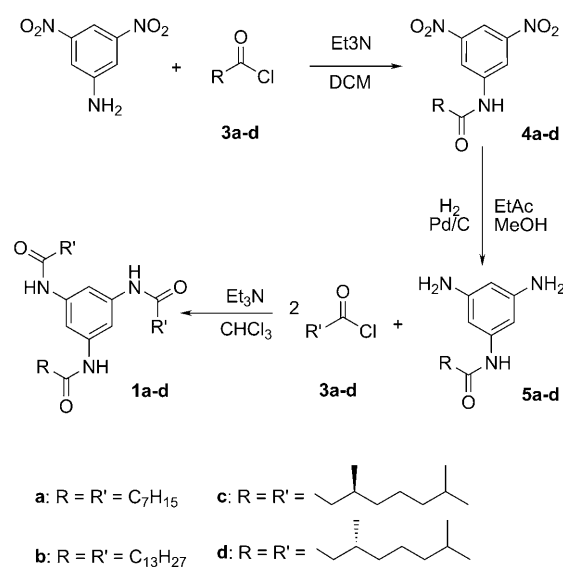


Figure 1. Texture obtained for compound **1c** after slow cooling from the isotropic state; $T = 224^\circ\text{C}$.

ences in the self-assembly behaviour of **1** and **2** was rationalised by using DFT calculations. Finally, we mixed C=O- and N-centred BTAs to evaluate whether alternating supramolecular block copolymers are accessible in this way, as a first step to increase complexity with a new level of understanding.

Results and Discussion

Synthesis: The synthetic approach to trialkyl substituted N-centred BTAs is depicted in Scheme 1. The procedure is an adaptation from literature.^[8] 3,5-Dinitroaniline was first re-



Scheme 1. Synthesis of N-centred BTAs **1a–d**.

acted with acid chlorides **3a–d** (octanoyl chloride, tridecanoyl chloride and (*R*)- or (*S*)-3,7-dimethyloctanoyl chloride, respectively) affording **4a–d**. We selected alkyl groups which differed in alkyl chain length (C₁₃H₂₇ and C₇H₁₅), in branching (3,7-dimethyloctanoyl) and in chirality ((*R*)-3,7-dimethyloctanoyl and (*S*)-3,7-dimethyloctanoyl) to assess the impact of side chains on the thermal behaviour and self-assembly properties. Catalytic reduction of the nitro group with H₂/Pd afforded the diamino derivatives **5a–d**. Compounds **5a–d** were reacted with the acid chlorides **3a–d** to afford the desired symmetrically substituted N-centred BTAs **1a–d**. After column chromatography, compounds **1a–d** were obtained in high purity as evidenced by ¹H and ¹³C NMR spectroscopy and Maldi-Tof-MS.

Solid-state properties of N-centred BTAs 1a–d: The effect of amide connectivity in BTAs was first evaluated in the solid state by employing DSC and POM; the data obtained were compared to those of C=O-BTA reference compounds **2a,b**. The thermal transitions observed in the second heating run in DSC are summarised in Table 1.

Table 1. Summary of the DSC and IR data of BTAs **1a–d** and **2a,b**.

	T [°C] ^[a] (ΔH [kJ mol ^{−1}]) ^[a]	ν_{NH} ^[b] [cm ^{−1}]	$\nu_{\text{C=O}}$ ^[b] [cm ^{−1}]	$\nu_{\text{C–N}}$ ^[b] [cm ^{−1}]
1a	K 174.9 (41.2) I	3271	1656/1614	1550
1b	K ₁ 94.6 (23.1) K ₂ 149.5 (38.1) I	3278 3310 ^[d]	1649/1607 1665/1605 ^[d]	1551 1536 ^[d]
1c	Col _{ho} 215.1 (15.3) I	3269 3250 ^[d]	1656/1614 1651 ^[d]	1550 1523 ^[d]
1d	Col _{ho} 218.0 (15.9) I	3272 3236 ^[e]	1656/1615 1640 ^[e]	1553 1557 ^[e]
2a ^[c]	K 19 (17) Col _{ho} 198 (8) I	3306 ^[f]	1644 ^[f]	1531 ^[f]
2b ^[c]	K 120 (13) Col _{ho} 235 (18) I	3223 ^[f]	1637 ^[f]	1564 ^[f]

[a] Data derived from the second heating run in DSC. [b] Measured at room temperature for an untreated sample. [c] Data obtained from reference [1d]. [d] IR data obtained at $T = 175^\circ\text{C}$. [e] IR data obtained directly after heating into the mesophase and fast cooling to RT. [f] IR data obtained at room temperature, for **2a** this corresponds to a non-helical arrangement of the hydrogen bonds.

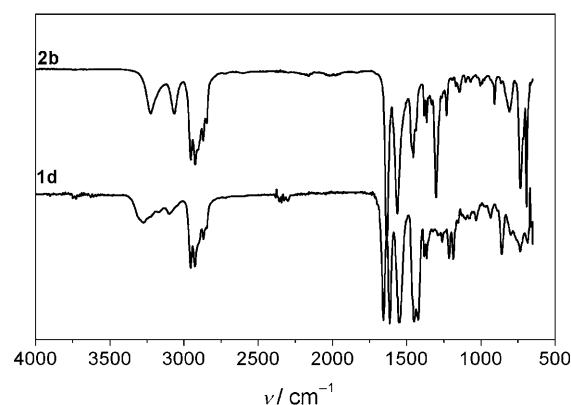
Previous research indicated that starting from a hexyl side chain, C=O-centred BTAs **2a,b** are liquid crystalline (LC) and that the LC phase is an ordered, columnar hexagonal phase (Col_{ho}) (Table 1).^[1d] In contrast to the C=O-centred BTAs, POM investigations on N-centred BTAs revealed that unbranched derivatives do not form a mesophase. Compounds **1a** and **1b** are crystalline solids that melt into an isotropic liquid (I) at 174.9 and 149.5°C, respectively. Increasing the bulkiness of the alkyl side chain is sufficient to induce an LC phase. Branched **1c** and **1d** exhibit a liquid crystalline phase from 91 to 224°C as evidenced by POM (Figure 1) and by the first heating run in DSC (ESI, Figure S1). Interestingly, the transition at 91°C does not reappear in the second heating run (Table 1), but a transition at around 8°C is observed, while the LC-to-I transition is observed at 215–218°C. The isotropisation temperature and concomitant enthalpy of branched N-centred BTA **1c,d** is similar to that of its C=O-centred counterpart **2b**.

X-ray diffraction measurements on a sample of (*S*)-**1c** unambiguously confirmed a hexagonally ordered, columnar mesophase (Col_{ho}) phase. At 160°C two features are detected in the wide-angle region: first, a sharp reflection that corresponds to a distance of 3.5 Å and is characteristic of the stacking of disc-like molecules; second, a broad diffuse halo, associated to a distance of about 5.0 Å, that arises from short-range interactions between the aliphatic chains as is typically observed in liquid crystalline phases. In the small-angle region, a set of three reflections at 16.3, 9.3 and 8.0 Å with spacings in the reciprocal ratio 2:√3:1 is consistent with a hexagonal packing of the columns. From these maxima we can deduce an intercolumnar distance of 18.8 Å.

More information on the organisation of the hydrogen bonds in the solid state of N-centred BTAs can be obtained by analysing the IR data. For C=O-centred BTAs, we established that IR spectroscopy is a sensitive technique to evaluate the nature of the intermolecular hydrogen bonding. Vibrations for the N–H stretch at $\approx 3240\text{ cm}^{-1}$, the C=O stretch at $\approx 1640\text{ cm}^{-1}$ and the amide II at $\approx 1560\text{ cm}^{-1}$ have been attributed to the presence of threefold, α -helical type

intermolecular hydrogen bonding between neighbouring molecules, while vibrations for the NH stretch at 3306 cm^{-1} and an amide II vibration at 1530 cm^{-1} are typical for a non-helical organisation of the hydrogen bonds.^[1d]

The IR data measured of virgin samples of N-centred BTAs **1a–d**, that is, after isolation and without any thermal treatment, are summarised in Table 1. In all cases, the NH stretch is found at 3270 cm^{-1} while two C=O stretch vibrations at about 1656 and 1615 cm^{-1} and an amide II vibration at approximately 1550 cm^{-1} are observed. To visualise the differences between chiral **1d** and **2b**, Figure 2 compares the

Figure 2. Comparison of the IR spectra of **1d** and **2b** at room temperature.

room temperature IR spectra of **2b** (in which threefold hydrogen bonding in a helical packing is present) and **1d**. There is less symmetry in the NH stretch vibration of **1d** and the splitting of the C=O vibration suggests that the hydrogen bonds are organised in a non-helical way. In fact, the IR trace of **1d** resembles the IR trace previously observed for compound **2a** at room temperature, where a non-helical arrangement of the hydrogen bonds was assigned.^[1d]

We then performed variable-temperature IR spectra of compound **1b** and **1d** in order to investigate differences in the hydrogen bonds as a function of temperature (see Table 2 and Figure S2 in the Supporting Information). Compound **1b** is a crystalline solid that melts at 149.5°C. The IR traces remain identical when heating the sample until the melting temperature is reached (Figure S2A in the Supporting Information). At 175°C, well above the melting point, the NH stretch is at 3310 cm^{-1} and the amide II is at 1536 cm^{-1} indicating the loss of hydrogen bonding (Table 1). In contrast, the NH stretch in case of **1d** lowers to a value of 3250 cm^{-1} at 175°C, while the carbonyl vibration merges

Table 2. Thermodynamic parameters of **1c** and **2b** ($c = 3 \cdot 10^{-5}\text{ M}$ in MCH) obtained by fitting the temperature-dependent data.

	h_e [kJ mol ^{−1}]	T_e [K]	K_a
1c	−50	328.5	2×10^{-5}
2b	−60	336.6	$\leq 10^{-5}/10^{-6}$

into one peak at 1651 cm^{-1} (Figure S2B in the Supporting Information). This observation, together with the fact that a Col_{ho} phase is present between 91 and 224°C in the first heating run, strongly points to a α -helical type packing of the hydrogen bonds in the liquid crystalline state of N-centred BTAs similar to the packing observed in C=O-centred BTA **2b**. After cooling to room temperature, the helical arrangement is retained but over time it slowly changes back into the non-helical packing pattern.

The data presented above indicate that N-centred BTAs have a complicated solid-state behaviour that depends strongly on the nature of the alkyl chain. Presumably, packing effects and maximisation of the crystal density govern the hydrogen bonding patterns in the solid state, an effect that was also observed previously for C=O-BTAs with short alkyl chains.^[1d] However, there are strong indications from IR in the Col_{ho} mesophase that the molecules organise into columns stabilised by threefold intermolecular hydrogen bonds. Unfortunately, to date, there is no crystal structure available for an N-centred derivative to validate this hypothesis. Therefore, we proceeded with studying the N-centred BTAs in dilute solution.

Self-assembly of N-centred BTAs in methylcyclohexane and methanol: The self-assembly of N-centred BTAs into dynamic supramolecular polymers was investigated by UV and CD spectroscopy in methylcyclohexane (MCH) and in methanol ($c=3\cdot 10^{-5}\text{ M}$). In methanol, N-centred BTAs are molecularly dissolved, while MCH favours stacking of the BTAs. This is evidenced by a strong Cotton effect in MCH (Figure 3A), while no Cotton effect is present in methanol. Moreover, the UV spectra in methanol and MCH differ: the λ_{max} in MCH is at 223 nm, while that in methanol is at 240 nm (Supporting Information, Figure S3). The blue shift upon aggregation has been observed previously for C=O-centred BTAs and is attributed to a decrease in conjugation between the benzene unit and the amide substituent, because of hydrogen bond formation. Mirror image CD spectra were obtained for the enantiomer pair **1c,d** in MCH with $\Delta\epsilon = -63.1\text{ L mol}^{-1}\text{ cm}$ for **1c** and $+62.3\text{ L mol}^{-1}\text{ cm}$ for **1d** at $\lambda = 233\text{ nm}$ (Figure 3B). These results point to aggregation of the different enantiomers in helical supramolecular polymers of opposite helicity.

Variable-temperature CD measurements were performed on compound **1c** in MCH ($c=3\cdot 10^{-5}\text{ M}$). The temperature was decreased from 90 to 20°C and the CD intensity was monitored at $\lambda = 233\text{ nm}$, the maximum of the Cotton effect. The CD effect decreases with an increase in temperature and disappears at 55°C . A plot of the CD intensity measured at 233 nm versus the temperature is given in Figure 3C. The curve shows two regimes; a nucleation regime, in which all molecules are molecularly dissolved (indicated by the absence of a CD effect) and an elongation regime in which the aggregate rapidly grows. Upon cooling, at a certain (concentration dependent) temperature a large enough nucleus is formed allowing the formation of an aggregate. Fitting the cooling curves to the nucleation-growth model of

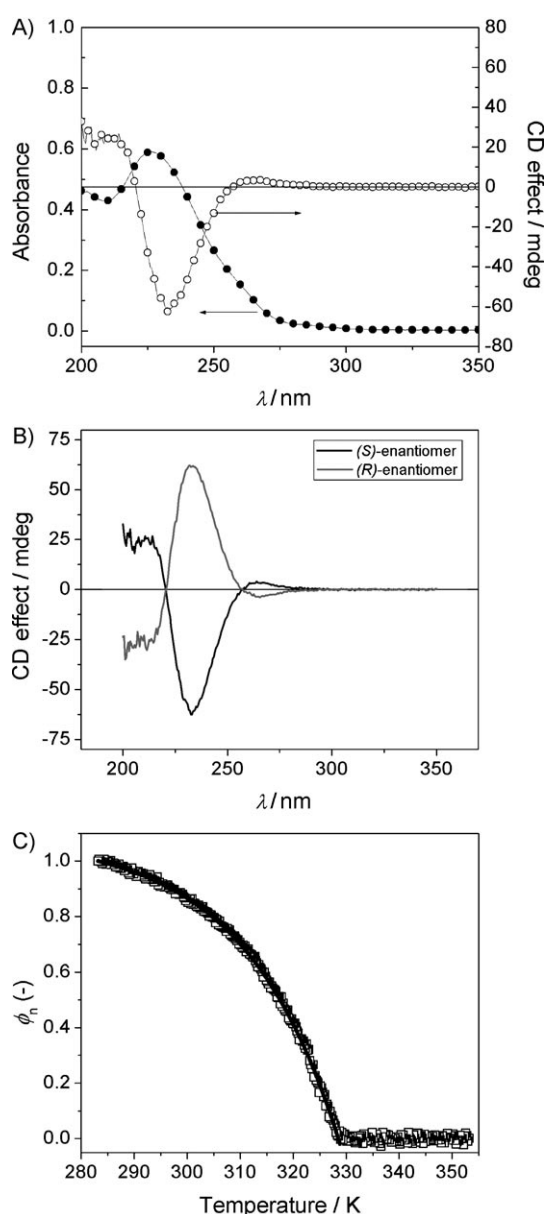


Figure 3. A) UV and CD spectra of **1c** in MCH, $c=3\cdot 10^{-5}\text{ M}$. B) Mirror image CD spectra of (*S*)-**1c** (black line) and (*R*)-**1d** (grey line), $c=3\cdot 10^{-5}$ in MCH. C) CD cooling curve of **1c** in MCH, $c=3\cdot 10^{-5}\text{ M}$, $\lambda = 233\text{ nm}$.

van der Schoot affords T_e (the elongation temperature) and h_e (the enthalpy release upon elongation).^[5b,9] Moreover, K_a —the equilibrium constant between the monomeric and the active state—can be derived and is a measure for the degree of cooperativity in the system. The T_e , h_e and K_a data are given Table 2 and compared to data previously derived for the C=O-centred BTA **2b**.^[5b] It is clear that the C=O-centred BTAs are more stable and aggregation results in a higher enthalpy release as evidenced by a higher T_e and h_e at identical concentration in MCH. Moreover, the aggregation of **1c** appears to be less cooperative than that of **2b** (Figure S4 in the Supporting Information), but unfortunately the values for K_a cannot be directly compared as they are determined at a different T_e .

Amplification of chirality in N-centred BTAs: When molecules of conflicting chiral information (i.e., *R* and *S* enantiomers) are mixed, the so-called majority rules effect is operative in C=O-centred BTAs. The majority rules effect states that the enantiomer present in the majority dictates the helical sense to which the minority enantiomer adjusts. In addition, adding small amounts of a chiral BTA to an achiral solution consisting of equal amounts of *P* and *M* helical supramolecular polymers results in stacks of either *P* or *M* helicity. This effect is commonly referred to as the sergeants-and-soldiers effect. Sergeants-and-soldiers (SaS) and Majority Rules (MR) experiments in C=O-centred BTAs showed a pronounced amplification of chirality effect, that is, the observed CD effect is much higher than expected based on the net enantiomeric excess (for the MR experiment) or the amount of chiral compound added (for the SaS experiment).

For the N-centred BTAs, chiral **1c**, the sergeant, was titrated into a solution of achiral **1b**, the soldier, and the CD-effect was followed as a function of the amount of chiral **1c** added (MCH, $c = 3 \times 10^{-5}$ M). Since achiral compounds have no preferred helicity, equal amounts of *P* and *M* helices are present and no CD effect is measured. The result of the titration is shown in Figure 4A. A similar experiment was then conducted using enantiomers **1c** and **1d** mixed in different ratios (Figure 4B). Clearly, in both cases the CD effect is not linear with respect to the enantiomeric excess

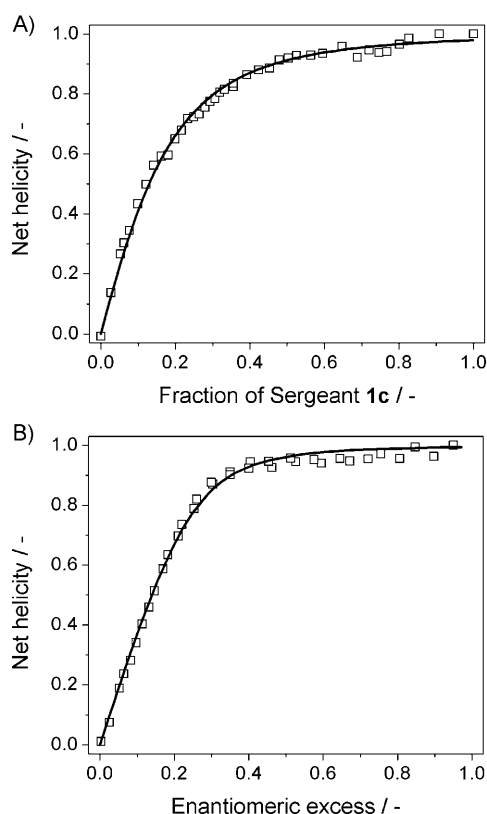


Figure 4. A) Results from a SaS experiment using **1a** and **1c** and B) results from a MR experiment using **1c** and **1d**. In all cases the Cotton effect is probed at 233 nm and $c = 3 \times 10^{-5}$ M in MCH.

(MR experiment) and the amount of sergeant added (the SaS experiment). This shows that amplification of chirality is indeed present in N-centred BTAs.

Theoretical models developed by van Gestel^[10] and van der Schoot^[11] allow us to quantify the energies that are involved in chiral amplification processes: the mismatch energy (E_M), that is, the penalty that is paid by the minority enantiomer to be present in a helix of its non-preferred sense and the helix reversal penalty (E_R), that is, the penalty that it cost for a helix to change its helical sense. Both energies are derived from experimental data. This model recently yielded values for E_M and E_R in bipyridine- and C=O-based BTAs.^[11,12] The results obtained for the N-centred BTAs **1** are summarised in Table 3 and compared to those

Table 3. Mismatch energy penalty (E_M) and helix reversal energy (E_R) for **1** and **2** in MCH ($c = 3 \times 10^{-5}$ M).

	1		2	
	E_M [kJ mol ⁻¹]	E_R [kJ mol ⁻¹]	E_M [kJ mol ⁻¹]	E_R [kJ mol ⁻¹]
SaS	> 0.5 ^[a]	7.3 ± 2.5	> 0.5 ^[a]	12.6 ± 2.0
MR	1.3 ± 0.4	12 ± 4	1.9 ± 0.2	15 ± 4

[a] Fitting the SaS data only allows to determine a lower limit for E_M .

obtained for C=O-centred BTA **2**. Both the mismatch penalty ($E_M = 1.3$ kJ mol⁻¹) and the helix reversal penalty ($E_R = 12$ kJ mol⁻¹) are lower in case of the N-centred BTA compared to the C=O-centred BTA ($E_M = 1.9$ kJ mol⁻¹ and $E_R = 15$ kJ mol⁻¹, respectively), showing that the degree to which amplification of chirality takes place is lower in case of N-centred BTAs. The difference may very well be related to the lower degree of cooperativity observed for the aggregation of N-centred BTAs. Unfortunately, to date there are very few examples known in literature where amplification of chirality is studied systematically in cooperative systems.^[11]

Origin of the differences between N-centred and C=O-centred BTAs: Most likely, the differences in aggregate stability can be attributed to differences in hydrogen-bonding strength between the different BTAs. However, estimations of the pK_a 's of the NH in **1** and **2** in DMSO show that these are rather similar.^[13] Therefore, one cannot rationalise, a priori, which hydrogen bond will be stronger. Because of the unavailability of a crystal structure of an N-centred BTA and to get more insight in the self-assembly behaviour of the N- and C=O-centred BTAs, DFT calculations were performed. In order to reduce the computational costs, the calculations were performed on oligomers and infinite chains of BTAs **3** and **4** (Figure 5), in which the long aliphatic side chains were replaced with by methyl groups.

Plane-wave DFT (PW-DFT) electronic-structure calculations were performed by using the VASP code, as it is well suited for studies of large periodic systems such as the hydrogen-bonded chains formed by BTAs.^[14] All DFT calculations were performed using the PBE exchange-correlation

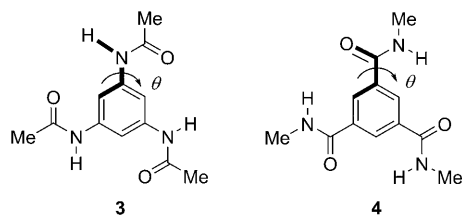


Figure 5. N-centred BTA **3** and C=O-centred BTA **4** used in the computational studies. The torsion angle θ for each BTA used to characterise the PW-DFT geometries is also shown.

functional^[15] that has been shown to reproduce hydrogen-bond lengths and energies with high accuracy.^[16] An advantage of PW-DFT is that it is inherently free from the basis-set superposition error (BSSE), because plane-wave basis sets describe any point in the periodic supercell with the same quality in contrast to Gaussian orbitals spanning only a local region.^[17]

Geometries of infinite chains of N-centred BTA **3** and C=O-centred BTA **4** were optimised by using the PW-DFT approach. Since PW-DFT calculations are of inherently periodic nature, an N- or C=O-centred BTA dimeric unit was placed in an ($a \times a \times c$) orthorhombic supercell. A vacuum layer ($a = 20 \text{ \AA}$) was added along the two directions perpendicular to the direction of the infinite chain in order to avoid spurious interactions between the periodic images of the system. Optimum lattice constants c equal to 7.20 and 7.40 \AA for **3** and **4**, respectively, were chosen from the minimisation of the total energy with respect to this parameter. Figure 6 shows the optimised geometry of the infinite, hy-

drogen-bonded chain of C=O-centred BTA **4** and the reported X-ray structure, we next investigated the differences between the optimised geometries of the infinite chains of C=O-centred BTA **4** and N-centred BTA **3**. Whereas the $C_a-C_a-C_c-O$ dihedral angle in the infinite chain of BTA **4** is -40.8° , the C_a-C_a-N-H dihedral angle (θ ; Figure 5) in the infinite chain of N-centred BTA **3** is -38.6° . Furthermore, the hydrogen-bond length (d_{N-O}) in the infinite helical chain of N-centred BTA **3** is somewhat longer (3.01 \AA) compared to that in the infinite helical chain of C=O-centred BTA **4** (2.98 \AA). This effect is more pronounced in the computed N-H...O distances (Figure 5). The longer hydrogen bond and smaller dihedral angle of the infinite chain of N-centred BTA **3** is expected to result in a lower cohesive energy per molecular unit compared to the infinite chain of C=O-centred BTA **4**. Indeed, the elongation enthalpies, a measure for the cohesive energy per molecular unit, obtained from the analysis of the temperature-dependent CD data in MCH suggests that the enthalpy release (h_e) for addition of a single monomer is higher for stacks of C=O-centred BTAs than stacks composed of N-centred BTAs by 10 kJ mol^{-1} .

This is in line with the differences in the computed average interaction energies in the supramolecular chains of **3** and **4** (Figure 6). The average interaction energy, that is cohesive energy, per molecular unit was evaluated as $\Delta E = (E_d^i - 2E_{\text{mon}}^i)/2$, in which E_d^i is the computed electronic energy of the unit cell containing two BTA monomers periodically repeated to yield the infinite BTA chain and E_{mon}^i is the electronic energy of the monomer computed at the same level of theory.^[18] The computed cohesive energy per molecule in the gas phase equals -73 kJ mol^{-1} and -41 kJ mol^{-1} for the infinite chains of C=O-centred **4** and N-centred **3** BTA, respectively. Hence, the order of stability as found

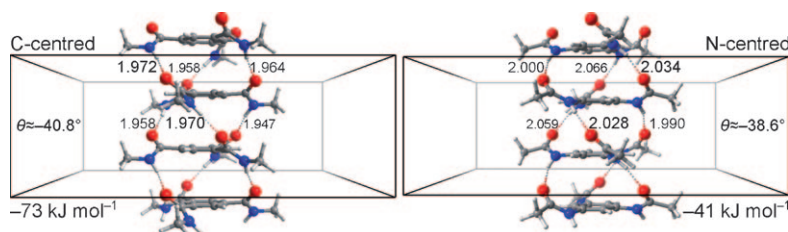


Figure 6. PW-DFT optimised structures and N-H...O hydrogen-bond lengths (\AA) of infinite chains of C=O-centred BTA **4** and N-centred BTA **3**. Energy values presented correspond to the average interaction energy (ΔE) between the monomers in the respective supramolecular ensemble.

drogen-bonded chains of BTAs **3** and **4**, while the relevant structural parameters are reported in Table 4 together with the structural parameters from the crystal structure of a C=O-centred BTA reported by Lightfoot et al.^[4a]

Table 4. Structural parameters of the optimised structures of infinite chains of BTAs **3** and **4** together with the structural parameters from the crystal structure reported by Lightfoot et al.^[4a]

Structure	θ [$^\circ$]	d_{O-N} [\AA]	d_{ring} [\AA]
PW-DFT infinite chain of BTA 3	-38.6	3.01	3.60
PW-DFT infinite chain of BTA 4	-40.8	2.98	3.70
crystal structure C=O-centred 4a	-41.5	2.97	3.62

using the PW-DFT calculations agrees with the order of stability as found from the analysis of the CD data.

As already mentioned, the pK_a 's of the NH in the N- and C=O-centred monomeric BTAs are very similar, indicating that the lower cohesive energy per molecular unit for infinite stacks of **3** with respect to **4** cannot solely be due to the stronger hydrogen bonds formed by the BTA monomer in the latter. Analysis of the hydrogen-bond length, which has been claimed^[19] to be a good measure of hydrogen-bond strength, in both optimised geometries shows that the hydrogen bonds in the C=O-centred infinite chain are somewhat shorter than in the N-centred infinite chain, although the difference is only minor (0.03 Å). Therefore, we hypothesised that the reduction in the computed cohesive energy per molecular unit as found for the infinite stacks of N-centred BTA **3** relative to **4** is primarily due to the differences in dipole–dipole interactions between the monomers, partially as a result of the smaller dihedral angle found in the infinite hydrogen bonded chains consisting of BTA **3**.

To correlate the observed difference in stability between C=O- and N-centred hydrogen-bonded supramolecular polymers to the structures of their respective monomers, we reasoned that the difference in stability of the two supramolecular polymers is caused by the higher energetic barrier for rotation of the C_a–C_a–N–H dihedral angle in the N-centred BTA monomer compared to rotation of the C_a–C_a–C_c–O dihedral angle in the C=O-centred BTA monomer. Upon formation of threefold hydrogen bonds in supramolecular polymers consisting of C=O- or N-centred BTAs, the amide group of the monomeric BTAs has to rotate out of the plane of the benzene ring. In order to explore the conformational change of the aromatic BTA amides **3** and **4** and the role of amide connectivity, torsional energy profiles were calculated for the torsions around all of the C_{aromatic}–C_{carbonyl} bonds of BTA **4** and all of the C_{aromatic}–N bonds of BTA **3** (Figure 5). The equilibrium geometries were obtained by full geometry optimisation at PBE/6-311G+(d,p) level of theory by using the Gaussian 03 program.^[20] Initially, torsional energy profiles were obtained by scanning the torsional potential surface in 5° increments at PBE/6-311G+(d,p) level of theory. At each scan point, all internal coordinates except the three torsional angles driving the scan were optimised. The calculated potential energy curves for **3** and **4** as a function of the dihedral angle θ are displayed in Figure 7. The equilibrium geometry of C=O-centred BTA **4** already shows a pronounced nonplanarity between the aromatic ring and the amide group. The amide groups in **4** are tilted out of plane by $\approx 12^\circ$. The deviation from planarity probably results from steric repulsion between the arene *ortho*-hydrogen atoms and the oxygen atoms of the carbonyl groups. DFT and MP2 calculations on the related compound N-methyl benzamide (NMB) conducted by Pophristic et al.^[21] and Vargas et al.^[22] indicate that the equilibrium geometry of NMB is also characterised by pronounced nonplanarity between the aromatic ring and the amide group. Furthermore, Vargas et al.^[22] analysed X-ray structures containing a phenyl ring attached to an amide C=O, in which both

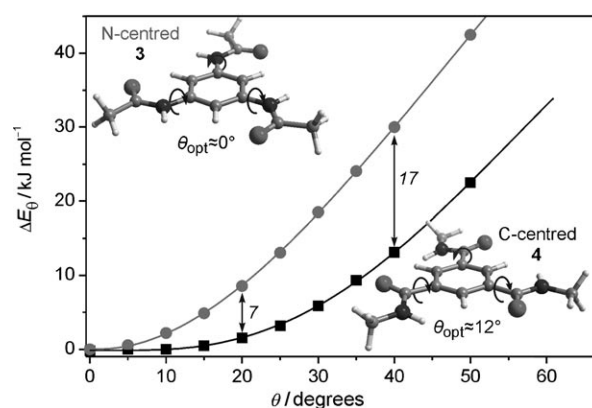


Figure 7. Potential energy profiles for torsion around the C_{aromatic}–C_{carbonyl} bond of C=O-centred BTA **4** and the C_{aromatic}–N bond of N-centred BTA **3** (PBE/6-311+G(d,p)). The energy profiles are obtained by scanning the torsional potential surface in increments of 5° for the C_a–C_a–C_c–O dihedral angle of **4** and C_a–C_a–N–H dihedral angle of **3**.

arene *ortho*-positions were occupied by hydrogen atoms and the nitrogen was substituted with a hydrogen atom and a C(sp₃) carbon. They found that the average dihedral angle in all the X-ray structures was $\theta \approx 22^\circ$.

In contrast, the equilibrium structure of N-centred BTA **3** is characterised by the amide group in the same plane as the benzene ($\theta \approx 0^\circ$). Previous DFT studies reported by Doerksen et al.^[23] on the related compound acetanilide, show that also in this structure the amide is in plane with the benzene ring. The steric repulsion between the arene *ortho*-protons and the smaller NH moiety in **3** is weaker as relative to that involving larger C=O group in **4**. In addition, the equilibrium conformation of N-centred BTA **4** shows an unusually short O...H–(C₆) intramolecular distance (2.18 Å), which matches known values^[14] for such hydrogen bonds. Such a weak hydrogen bond may play a role in the stabilisation of the planar geometry of N-centred BTA **4**. The observed differences in the computed torsional potential surface for **3** and **4** are influenced by the conjugation of the amide and arene π orbitals, steric repulsions with arene *ortho*-hydrogen atoms and weak intramolecular hydrogen bonding.

As a result of the differences in the steric repulsion between the arene *ortho*-protons and the amide H and O atoms in BTA **4** and BTA **3**, respectively, rotation of the amide in N-centred BTAs is substantially hindered as compared to that in the C=O-centred BTAs (Figure 7). Indeed, for a dihedral angle of 40°, which corresponds to the value obtained in infinite chains of BTAs **3** and **4**, the N-centred BTA is 18 kJ mol^{–1} higher in energy. Thus stronger and more unfavourable deformations of the N-centred BTA monomers are required upon its addition to a supramolecular polymer consisting of N-centred molecules. This results in the less favourable supramolecular polymerisation process of the N-centred BTAs as compared to the C-centred isomers. Furthermore, rotation of the amide groups in the C=O-centred BTA **4** results in a somewhat larger dipole moment as compared to that in the N-centred BTA mono-

mer **3** at all values of the dihedral angle θ (Figure 8). The larger dipole in the perturbed structures of **4** enhances the dipole–dipole interactions in the corresponding supramolec-

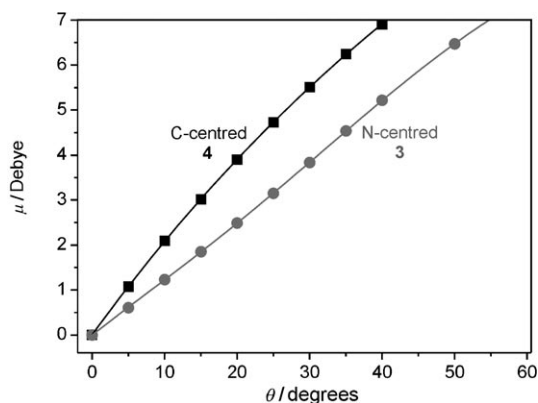


Figure 8. Evolution of the dipole moment in the N-centred **3** and C=O-centred **4** BTA monomers upon the increase of the dihedral angle around the $C_{\text{aromatic}}-C_{\text{carbonyl}}$ bond and the $C_{\text{aromatic}}-\text{NH}$ bond, respectively (PBE/6-311+G(d,p)).

ular structures and hence further stabilises supramolecular polymers consisting of C=O-centred BTAs as compared to those formed from N-centred BTAs. One expects that the nonplanarity of the monomeric BTA units gradually increases at the initial stage of the supramolecular polymer growth and finally reaches the limiting value computed for the infinite BTA chains. The resulting evolution of the macrodipole as a function of stack size influences the cooperativity in the growth of the resulting supramolecular polymer.^[25] We therefore speculate that a difference between the evolution of the macrodipole as a function of chain length may explain the differences in cooperativity observed for the N- and C=O-centred BTAs.

Mixed stacks of N-centred and C=O-centred BTAs: Both N- and C=O-centred BTAs form columnar aggregates in dilute solutions stabilised by means of threefold intermolecular hydrogen bonding, and the results discussed above indicate that the aggregation and degree of amplification of chirality is weaker in case of N-centred BTAs. An intriguing question is if the different hydrogen-bond strengths can be utilised in making alternating supramolecular block copolymers, an observation previously made in two component organogel systems in which amide- and urea-based BTAs were found to form a more stable gel in a mixed system.^[26]

To investigate the feasibility of this, we performed mixing experiments of chiral **1c** and achiral **2a** and measured the CD spectra as a function of chiral **1c** added. As depicted in Figure 9A, achiral **2a** shows no CD effect, but upon addition of only 5% of **1c**, there is a fast increase of the CD effect. The shape of the CD spectrum between 0 and 20% **1c** added is typical for that of a C=O-centred BTA.^[5b] Starting from around 20% **1c**, the shape of the CD curve changes into a CD curve typical of an N-centred BTA with

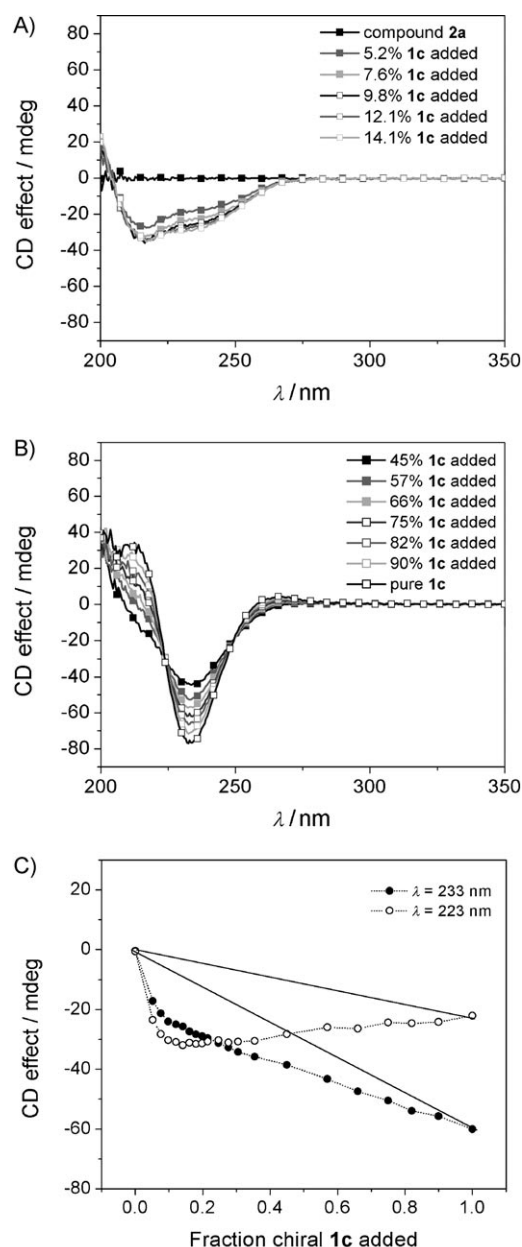


Figure 9. A) CD spectra of **1c** added to achiral **2a** at low fractions of **1c** (MCH, $c=3\cdot 10^{-5}$ M). B) CD spectra of **1c** added to achiral **2a** at high fractions of **1c** (MCH, $c=3\cdot 10^{-5}$ M). C) CD effect at 223 and 233 nm as a function of the amount of chiral **1c** added to achiral **2a** (MCH, $c=3\cdot 10^{-5}$ M).

a λ_{max} at 233 nm (Figure 9B, see the Supporting Information for more spectra). Because of the changes in the shape of the CD spectra it is difficult to select a wavelength at which to probe the amplification of chirality. We selected $\lambda=223$ and 233 nm, at which C=O- and N-centred BTAs have a maximal Cotton effect, respectively, as the wavelength of choice and plotted the CD intensity as a function of chiral **1c** added. As seen in Figure 9C, there is a clear deviation from linearity when probing the CD effect at $\lambda=223$ and 233 nm. Remarkably, at $\lambda=223$ nm the levelling off of the CD effect is observed at only 10% of the added chiral com-

ponent and the $\Delta\epsilon$ remains more or less constant at $-30 \text{ L mol}^{-1} \text{ cm}^{-1}$. This value is in close agreement with a fully homochiral C=O-centred BTA stack for which $\Delta\epsilon$ values are typically around $-40 \text{ L mol}^{-1} \text{ cm}^{-1}$. At $\lambda = 233 \text{ nm}$, the increase is more gradual and no levelling off in the CD-effect is observed, which is quite similar to the SaS experiment conducted with chiral **1c** and achiral **1b**. The reverse experiment, namely adding achiral C=O-centred **2b** to achiral N-centred **1b**, was more difficult because of the poor solubility of **1b** in MCH at room temperature (see Figure S5 and S6 in the Supporting Information for additional data), but a clear deviation from linearity was observed also in this case. Although this is no definite proof of an alternating supramolecular block copolymer, it is clear that mixed stacks are formed.

Conclusion

Several N-centred benzene-1,3,5-tricarboxamides (N-BTAs) comprising chiral and achiral alkyl substituents were synthesised and their solid-state behaviour was studied using DSC, POM and X-ray diffraction. This revealed that the chiral N-BTA derivatives with a branched 3,7-dimethyloctanoyl chain are liquid crystalline and the mesophase can be assigned as Col_{ho} . In contrast, N-BTA derivatives with octanoyl and tetradecanoyl side chains lack a mesophase and are obtained as crystalline compounds. Variable-temperature IR spectroscopy confirmed the presence of threefold, intermolecular hydrogen bonding between neighbouring molecules in the mesophase. In the crystalline state at room temperature, on the other hand, a more complicated organisation of the hydrogen bonds between the molecules was observed.

UV and CD spectroscopy on dilute solutions of N-BTAs revealed that the self-assembly into supramolecular polymers is cooperative. Similar to the C=O-centred BTAs, N-BTA molecules form columnar stacks with a preferred helicity when a chiral alkyl chain was used. Both the sergeants-and-soldiers as well as the majority-rules principles are operative in stacks of N-BTAs. Interestingly, mixed stacks of N- and C=O-BTAs were formed in dilute solution, suggesting that such a system is thermodynamically more stable than separate stacks of N- and C=O-BTAs.

The self-assembly of N-BTAs resembles closely that of their C=O-centred counterparts, with the exception that aggregation is weaker and amplification of chirality is less pronounced. DFT calculations revealed that there is a higher energy penalty for the rotation around the Ph-NH bond compared to the Ph-CO bond in the monomer. Therefore, more unfavourable deformations of the N-BTA are required upon its addition to a growing supramolecular polymer. This effect along with weaker dipole-dipole interactions due to the lower dipole moment of the deformed monomers and weaker intermolecular hydrogen bonding in the supramolecular polymers result in less favourable polymerisation pro-

cess and rationalise the decreased stability of N-BTA aggregates with respect to C=O-BTA ones.

The lower cooperativity in the self-assembly of N-centred BTAs relative to that of the C=O-centred BTAs may cause the lower degree of amplification of chirality observed. A more in-depth theoretical investigation on the origin of the cooperativity and amplification of chirality in the N- and C=O-centred BTAs will be subject of future work. We anticipate that the results will allow understanding these phenomena at the fundamental level.

Experimental Section

Materials: (*R*)-(+)-Citronellic acid and (*S*)-(–)-citronellic acid were purchased from Aldrich and converted into the corresponding (*R*)- and (*S*)-3,7-dimethyloctanoic acid according to a described procedure.^[27] Reference compounds **2a,b** were prepared as described previously.^[14] All solvents were obtained from Biosolve, except for DMSO (Acros) and spectrophotometric grade methylcyclohexane (Aldrich). All other chemicals were obtained from either Acros or Aldrich. Dry dichloromethane was tapped off a distillation setup which contained molsieves, CHCl_3 was dried over molsieves and triethylamine was stored on KOH pellets. All other chemicals were used as received.

Methods: UV/Vis and circular dichroism measurements were performed on a Jasco J-815 spectropolarimeter, for which the sensitivity, time constants and scan rates were chosen appropriately. Corresponding temperature-dependent measurements were performed with a PFD-425S/15 Peltier-type temperature controller with a temperature range of 263–383 K and adjustable temperature slope, in all cases a temperature slope of 1 K min^{-1} was used. In all other measurements the temperature was set at 20°C . In all experiments the linear dichroism was also measured and in all cases no linear dichroism was observed. Separate UV/Vis spectra were obtained from a Perkin-Elmer UV/vis spectrometer Lambda 40 at 20°C . Cells with an optical path length of 1 cm were employed and spectroscopic grade solvents were employed. Solutions were prepared by weighing in the necessary amount of compound for a given concentration and transferring it to a volumetric flask. Then the flask was filled three-quarters filled with the spectroscopic grade solvent and put in an oscillation bath at 40°C for 45 min, after which the flask was allowed to cool down and filled up to its meniscus. The $\Delta\epsilon = \text{CD effect}/(32980cl)$ in which c is the concentration in mol L^{-1} and l is the optical path length in cm. ^1H NMR and ^{13}C NMR measurements were conducted on a Varian Mercury 200 MHz and/or a Varian Gemini 400 MHz. Proton chemical shifts are reported in ppm downfield from tetramethylsilane (TMS). Carbon chemical shifts are reported using the resonance of CDCl_3 as internal standard. Maldi-TOF-MS were acquired using a Perserptive Biosystem Voyager-DE PRO spectrometer. In all cases, α -cyano-4-hydroxycinnamic acid was employed as the matrix material. IR spectra were recorded on a Perkin-Elmer spectrum 1 using a universal ATR. Variable-temperature IR spectra were recorded on an Excalibur FTS 3000 MX FT-IR from Biorad. Polarisation optical microscopy measurements were done using a Jenaval polarisation microscope equipped with a Linkam THMS 600 heating device, with crossed polarisers. The thermal transitions were determined with DSC by using a Perkin-Elmer Pyris 1 DSC under a nitrogen atmosphere with heating and cooling rates of 10 K min^{-1} . The T_g was determined with heating and cooling rates of 40 K min^{-1} . The XRD patterns were obtained with a pinhole camera (Anton-Paar) operating with a point-focused Ni-filtered $\text{CuK}\alpha$ beam. In this setup, the samples are held in Lindemann glass capillaries (0.9 mm diameter). The capillary axis is perpendicular to the X-ray beam and the pattern is collected on a flat photographic film perpendicular to the beam. Spacings are obtained via Bragg's law ($n\lambda = 2d\sin\theta$).

Procedure for the synthesis of acid chlorides 3c,d: (*S*)-3,7-Dimethyloctanoic acid (2.76 g, 16.00 mmol) was dissolved in dry CH_2Cl_2 (30 mL) under an argon atmosphere and cooled on an ice bath. A solution of oxalyl

chloride (1.65 mL, 19.22 mmol, 1.2 equiv) in dry CH_2Cl_2 (20 mL) was added dropwise and the solution was stirred under an argon atmosphere at room temperature for an additional 3 h. Evaporation of the solvent and the excess oxalylchloride in vacuo yielded **3c** as a yellow oil (2.78 g, 14.6 mmol, 92% yield), which was used as such. ^1H NMR (CDCl_3): δ = 2.88 (dd, 1H; $(\text{COOH})\text{CH}_2$), 2.71 (dd, 1H; $(\text{COOH})\text{CH}_2$), 2.10–2.08 (m, 1H; $(\text{CH}_2)_2\text{CHCH}_3$), 1.59–1.51 (m, 1H; $\text{CH}_2\text{CH}(\text{CH}_3)_2$), 1.36–1.14 (m, 6H; $-\text{CH}_2-$), 1.00 (d, 3H; CHCH_3), 0.89 ppm (d, 6H; $\text{CH}(\text{CH}_3)_2$) ppm; FT-IR: $\tilde{\nu}$ = 2957, 2930, 2870, 1799, 1464, 1384, 985, 967, 929 cm^{-1} . Acid chloride **3d** was obtained in an identical procedure.

General procedure for the synthesis of 3,5-dinitrobenzene-1-monocarboxamide (4a–d): 3,5-Dinitroaniline (1 equiv) was dissolved in dry CH_2Cl_2 at a concentration of 0.5 M and triethylamine (Et_3N ; 1.5 equiv) was added. The solution was stirred at 0°C under a nitrogen atmosphere. The appropriate acid chloride **3a–d** (1.2 equiv) was dissolved in dry CH_2Cl_2 at a concentration of 0.5 M and added slowly to the amine solution. After the addition was complete, stirring was continued overnight at room temperature. The solvents were removed in vacuo and the crude product was diluted to 0.1 M with chloroform. The solution was sequentially washed with 1 M HCl, water, 0.5 M NaOH aqueous solution, water and brine. The solution was dried with MgSO_4 and the solvent was removed in vacuo. The resulting crude compound was purified with column chromatography using silica as the stationary phase. For **4a** the eluent was chloroform/methanol 99:1, for **4b–d** the eluent was dimethoxyethane/heptane 1:5. The yields were between 36 and 50% after column chromatography. **4a**: ^1H NMR (CDCl_3): δ = 8.81 (t, 2H; Ar-H), 8.72 (t, 1H; Ar-H), 8.16 (brs, 1H; N-H), 2.50 (t, 2H; $\text{CO}-\text{CH}_2$), 1.66 (q, 2H; $\text{COCH}_2-\text{CH}_2$), 1.30–1.10 (m, 8H; CH_2), 0.88 ppm (t, 3H; CH_3). **4b**: ^1H NMR (CDCl_3): δ = 8.80 (t, 2H; Ar-H), 8.74 (t, 1H; Ar-H), 7.66 (brs, 1H; N-H), 2.46 (t, 2H; COCH_2), 1.78 (q, 2H; $\text{COCH}_2-\text{CH}_2$), 1.26–1.10 (m, 20H; CH_2), 0.88 ppm (t, 3H; CH_3). **4c,d**: ^1H NMR (CDCl_3): δ = 8.80 (t, 2H; Ar-H), 8.74 (t, 1H; Ar-H), 7.76 (brs, 1H; N-H), 2.36–2.18 (dd, 2H; COCH_2), 2.08–2.06 (m, 1H; $\text{CH}-(\text{CH}_3)_2$), 1.56–1.17 (m, 7H; $\text{CH}-(\text{CH}_3)_2$ and CH_2), 1.00 (d, 3H; $\text{CH}-(\text{CH}_3)_2$), 0.86 ppm (d, 6H; $\text{CH}-(\text{CH}_3)_2$).

General procedure for the synthesis of 3,5-diaminobenzene-1-monocarboxamide (5a–d): The appropriate dinitro compound (**4a–d**) was dissolved in ethyl acetate/methanol (1/1 v/v) in a concentration of 0.05 M and degassed with nitrogen. A catalytic amount of palladium on carbon (10%) was added and the solution was hydrogenated using a Parr apparatus until no more hydrogen was consumed. After that, the solution was filtered and the residue was washed with methanol. The solvents were removed in vacuo and the product was isolated in nearly quantitative yield and used the same day for the next step. **5a**: ^1H NMR (CDCl_3 + drop of $[\text{D}_6]\text{DMSO}$): δ = 9.20 (s, 1H; NH), 6.21 (s, 2H; Ar-H), 5.80 (brs, 4H; NH_2), 5.60 (t, 1H; Ar-H), 2.20 (t, 2H; COCH_2), 1.65 (q, 2H; $\text{COCH}_2-\text{CH}_2$), 1.26–1.10 (m, 8H; CH_2), 0.90 ppm (t, 3H; CH_3). **5b**: ^1H NMR (CDCl_3): δ = 7.21 (brs, 1H; N-H), 6.34 (t, 2H; Ar-H), 5.79 (t, 1H; Ar-H), 2.52 (t, 2H; COCH_2), 1.65 (t, 2H; $\text{COCH}_2-\text{CH}_2$), 1.26–1.10 (m, 2H; CH_2), 0.90 ppm (t, 3H; CH_3). **5c,d**: ^1H NMR (CDCl_3): δ = 7.21 (brs, 1H; N-H), 6.34 (t, 2H; Ar-H), 5.79 (t, 1H; Ar-H), 3.40 (brs, 4H; NH_2), 2.40–2.20 (dd, 2H; COCH_2), 2.10–2.08 (m, 1H; $(\text{CH}_2)_2\text{CH}(\text{CH}_3)$), 1.59–1.14 (m, 7H; $\text{CH}_2\text{CH}(\text{CH}_3)_2$ and $-\text{CH}_2-$), 1.00 (d, 3H; CHCH_3), 0.89 ppm (d, 6H; $\text{CH}(\text{CH}_3)_2$).

General procedure for the synthesis of N-centred BTAs 1a–d: The same procedure as described for compounds **4a–d** was carried out, with the difference that the solvent employed was dry chloroform and the appropriate acid chloride was added in 2.5 equivalents. The crude product was purified with column chromatography using silica as the stationary phase. For **1a** the eluent employed was chloroform/methanol 99:1, for **1b–d**, chloroform/ethylacetate 9:1 with a gradient to 8:2 was used. The yields after purification were typically around 30–50%.

Compound **1a** was obtained as a white solid. ^1H NMR (CDCl_3): δ = 7.66 (s, 3H; Ar-H), 7.28 (s, 3H; N-H), 2.31 (t, 6H; COCH_2), 1.69 (q, 6H; $\text{COCH}_2-\text{CH}_2$), 1.38–1.25 (m, 24H; CH_2), 0.88 (t, 9H; CH_3); ^{13}C NMR (CDCl_3): δ = 171.8 (C=O), 139.0 (Ar-C-N), 105.8 (Ar-C), 37.9, 31.6, 29.2, 29.0, 25.6, 22.6, 14.0 ppm; MALDI-TOF-MS: m/z observed: 524.49 Da [$M + \text{Na}$] $^+$; calcd: 501 Da.

Compound **1b** was obtained as a white solid. ^1H NMR (CDCl_3): δ = 7.65 (s, 3H; Ar-H), 7.17 (s, 3H; N-H), 2.31 (t, 6H; COCH_2), 1.69 (q, 6H; $\text{COCH}_2-\text{CH}_2$), 1.39–1.21 (m, 60H; CH_2), 0.88 ppm (t, 9H; CH_3); ^{13}C NMR (CDCl_3): δ = 187.0 (C=O), 133.3 (Ar-C-N), 105.4 (Ar-C), 67.4, 59.2, 53.5, 44.4, 37.9, 31.9, 29.6, 29.5, 29.3, 25.6, 22.7, 14.9, 14.1 ppm; MALDI-TOF-MS: m/z observed: 776.59 Da [$M + \text{Na}$] $^+$; calcd: 753 Da.

Compound **1c** was obtained as a sticky white solid. ^1H NMR (CDCl_3): δ = 7.68 (s, 3H; Ar-H), 7.44 (s, 3H; N-H), 2.34–1.99 (m, 6H; COCH_2), 1.69 (q, 6H; $\text{COCH}_2-\text{CH}_2$), 1.37–1.12 (m, 18H; CH_2), 0.97 (d, 9H; CH_3), 0.85 ppm (t, 18H; CH_3); ^{13}C NMR (CDCl_3): δ = 171.4 (C=O), 138.9 (Ar-C-N), 106.1 (Ar-C), 45.7, 39.0, 37.0, 30.9, 27.9, 24.7, 22.7, 22.5, 19.6 ppm; MALDI-TOF-MS: m/z observed: 608.52 Da [$M + \text{Na}$] $^+$; calcd: 585 Da.

Compound **1d** was obtained as a sticky white solid. ^1H NMR (CDCl_3): δ = 7.68 (s, 3H; Ar-H), 7.38 (s, 3H; N-H), 2.34–1.97 (m, 6H; COCH_2), 1.52 (q, 6H; $\text{COCH}_2-\text{CH}_2$), 1.39–1.12 (m, 18H; CH_2), 0.95 (d, 9H; CH_3), 0.85 ppm (t, 18H; CH_3); ^{13}C NMR (CDCl_3): δ = 171.4 (C=O), 138.9 (Ar-C-N), 105.9 (Ar-C), 45.7, 39.0, 37.0, 31.0, 27.9, 24.7, 22.7, 22.5, 19.6 ppm; MALDI-TOF-MS: m/z observed: 608.44 Da [$M + \text{Na}$] $^+$; calcd: 585 Da.

Computational details: Quantum chemical calculations on both the periodic chains of BTA or BTA monomers were performed within density functional theory with the gradient-corrected PBE^[15] exchange-correlation functional. Electronic structure calculations on the infinite BTA chains and related calculations on the monomeric species were carried out within the plane-wave DFT (PW-DFT) approach using the Vienna ab initio simulation package (VASP).^[14] The projected augmented wave (PAW) method^[28,29] was used to describe the electron-ion interactions and for valence electrons a plane-wave basis set was employed. During the geometry optimisation the energy cut-off was set to 400 eV. Total electronic energies used to estimate binding energies within the supramolecular ensemble were refined by performing single-point calculations on the optimised structures with higher energy cut-off of 600 eV. The Brillouin zone sampling was restricted to the Γ point.^[30] Full geometry optimisations were performed for each structure with the fixed cell parameters using a conjugate gradient algorithm. Convergence was assumed to be reached when the forces on each atom were below 0.02 eV \AA^{-1} . One-dimensional periodicity in the BTA chains was modelled by using a supercell approach. The elementary molecular unit of such chains that is a BTA dimer was periodically repeated in the direction of c vector of the orthorhombic unit cell. To minimise possible artificial interactions between the periodic images in a and b directions, the respective cell vectors were set to 20 \AA to assure a ≈ 10 \AA vacuum layer between the BTA chains. The unit cell size in the direction of the c vector was chosen based on the scan of the potential energy for the 1D periodic model with respect to this parameter. The minimum energy structures were obtained for c = 7.2 and 7.4 \AA for N-centred **3** and C=O-centred **4** BTA chains, respectively. The resulting parameters of the unit cells were $a=b=20$ \AA and $c=7.2$ and 7.4 \AA for N-centred **3** and C=O-centred **4** BTA chains, respectively. Monomeric BTA species were represented within the same periodic code and level of theory as the chain models by surrounding the molecular species with vacuum in a $20 \times 20 \times 20$ \AA^3 supercell.

Conformational study of monomeric BTA species was performed by using Gaussian 03 program package.^[20] Full geometry optimisations and partial geometry optimisations with fixed values of intramolecular dihedral angles were performed at the PBE/6-311+G(d,p) level of theory.

Acknowledgements

The authors would like to thank Koen Pieterse for his help with initial calculations and art-work and NOW and NRSC-C for financial support. The National Computing Facilities Foundation (NCF) is acknowledged for providing computational resources, with financial support from NOW (SH-125-08).

- [1] a) Y. Matsunaga, N. Miyajima, Y. Nakayasu, S. Sakai, M. Yonenaga, *Bull. Chem. Soc. Jpn.* **1988**, *61*, 207–210; b) Y. Matsunaga, Y. Nakayasu, S. Sakai, M. Yonenaga, *Mol. Cryst. Liq. Cryst.* **1986**, *141*, 327–333; c) Y. Kobayashi, Y. Matsunaga, *Bull. Chem. Soc. Jpn.* **1987**, *60*, 3515–3518; d) P. J. M. Stals, M. M. J. Smulders, R. Martín-Rapún, A. R. A. Palmans, E. W. Meijer, *Chem. Eur. J.* **2009**, *15*, 2071–2080.
- [2] a) K. Hanabusa, A. Kawamaki, M. Kimura, H. Shirai, *Chem. Lett.* **1997**, 191–192; b) K. Hanabusa, C. Koto, M. Kimura, H. Shirai, A. Kakehi, *Chem. Lett.* **1997**, 429–430; c) D. Ogata, T. Shikata, K. Hanabusa, *J. Phys. Chem. B* **2004**, *108*, 15503–15510; d) A. Sakamoto, D. Ogata, T. Shikata, K. Hanabusa, *Macromolecules* **2005**, *38*, 8983–8986; e) A. Sakamoto, D. Ogata, T. Shikata, O. Urakawa, K. Hanabusa, *Polymer* **2006**, *47*, 956–960; f) T. Shikata, D. Ogata, K. Hanabusa, *J. Phys. Chem. B* **2004**, *108*, 508–514; g) T. Shikata, Y. Kuruma, A. Sakamoto, K. Hanabusa, *J. Phys. Chem. B* **2008**, *112*, 16393–16402.
- [3] a) J. Roosma, T. Mes, P. Leclère, A. R. A. Palmans, E. W. Meijer, *J. Am. Chem. Soc.* **2008**, *130*, 1120–1121; b) C. F. C. Fitié, I. Tomatsu, D. Byelov, W. H. de Jeu, R. P. Sijbesma, *Chem. Mater.* **2008**, *20*, 2394–2404; c) R. van Hameren, P. Schön, A. M. van Buul, J. Hoogboom, S. V. Lazarenko, J. W. Gerritsen, H. Engelkamp, P. C. M. Christianen, H. A. Heus, J. C. Maan, T. Rasing, S. Speller, A. E. Rowan, J. A. A. W. Elemans, R. J. M. Nolte, *Science* **2006**, *314*, 1433–1436; d) I. Paraschiv, M. Giesbers, B. van Lagen, F. C. Grozema, R. D. Abellon, L. D. A. Siebbeles, A. T. M. Marcelis, H. Zuilhof, E. J. R. Sudhölter, *Chem. Mater.* **2006**, *18*, 968–974.
- [4] a) M. P. Lightfoot, F. S. Mair, R. G. Pritchard, J. E. Warren, *Chem. Commun.* **1999**, 1945–1946; b) P. P. Bose, M. G. B. Drew, A. K. Das, A. Banerjee, *Chem. Commun.* **2006**, 3196–3198.
- [5] a) L. Brunsveld, A. P. H. J. Schenning, M. A. C. Broeren, H. M. Janssen, J. A. J. M. Vekemans, E. W. Meijer, *Chem. Lett.* **2000**, 292–293; b) M. M. J. Smulders, A. P. H. J. Schenning, E. W. Meijer, *J. Am. Chem. Soc.* **2008**, *130*, 606–611.
- [6] M. Blomenhofer, S. Ganzleben, D. Hanft, H.-W. Schmidt, M. Kristiansen, P. Smith, K. Stoll, D. Mader, K. Hoffmann, *Macromolecules* **2005**, *38*, 3688–3695.
- [7] J. van Herrikhuyzen, P. Jonkheijm, A. P. H. J. Schenning, E. W. Meijer, *Org. Biomol. Chem.* **2006**, *4*, 1539–1545.
- [8] J. J. van Gorp, J. A. J. M. Vekemans, E. W. Meijer, *Mol. Cryst. Liq. Cryst.* **2003**, *397*, 191–205.
- [9] P. Jonkheijm, P. van der Schoot, A. P. H. J. Schenning, E. W. Meijer, *Science* **2006**, *313*, 80–83.
- [10] J. van Gestel, *Macromolecules* **2004**, *37*, 3894–3898.
- [11] M. M. J. Smulders, I. A. W. Filot, J. M. A. Leenders, P. van der Schoot, A. R. A. Palmans, A. P. H. J. Schenning, E. W. Meijer, unpublished results.
- [12] J. van Gestel, A. R. A. Palmans, B. Titulaer, J. A. J. M. Vekemans, E. W. Meijer, *J. Am. Chem. Soc.* **2005**, *127*, 5490–5494.
- [13] The pK_a 's of Ph-NHCO-CH₃ and Ph-CONH₂ measured in DMSO are 21.45 and 23.35, respectively. See F. G. Bordwell, D. Algrim, *J. Org. Chem.* **1976**, *41*, 2507–2508.
- [14] a) G. Kresse, J. Furtmüller, *Phys. Rev. B* **1996**, *54*, 11169–11186; b) G. Kresse, J. Furtmüller, *J. Comp. Mater. Sci.* **1996**, *6*, 15–50.
- [15] J. P. Perdew, K. Burke, M. Ernzerhof, *Phys. Rev. Lett.* **1996**, *77*, 3865–3868.
- [16] a) J. Ireta, J. Neugebauer, M. Scheffler, *J. Phys. Chem. A* **2004**, *108*, 5692; b) J. Ireta, J. Neugebauer, M. Scheffler, A. Rojo, M. Galván, *J. Phys. Chem. B* **2003**, *107*, 1432–1437; c) C. Tuma, ; A. D. Boese, N. C. Handy, *Phys. Chem. Chem. Phys.* **1999**, *1*, 3939–3947; d) R. Kaschner, D. Hohl, *J. Phys. Chem. A* **1998**, *102*, 5111–5116; e) T. van der Wijst, C. Fonseca-Guerra, M. Swart, F. M. Bickelhaupt, *Chem. Phys. Lett.* **2006**, *426*, 415–421; f) D. R. Hamann, *Phys. Rev. B* **1997**, *55*, R10157–R10160; g) J. A. Frey, S. Leutwyler, *J. Phys. Chem. A* **2006**, *110*, 12512–12518; h) Y. Zhao, D. G. Truhlar, *J. Chem. Theory Comput.* **2007**, *3*, 289–300.
- [17] R. S. Fellers, D. Barsky, F. Gygi, M. Colvin, *Chem. Phys. Lett.* **1999**, *312*, 548–555.
- [18] A. Rochefort, E. Bayard, D. Hadji-Messaoud, *Adv. Mater.* **2007**, *19*, 1992–1995.
- [19] a) S. J. Grabowski, *J. Phys. Chem. A* **2000**, *104*, 5551–5557; b) S. J. Grabowski, *Chem. Phys. Lett.* **1999**, *312*, 542–547; c) M. Rozenberg, A. Loewenschuss, Y. Marcus, *Phys. Chem. Chem. Phys.* **2000**, *2*, 2699–2702.
- [20] Gaussian 03, Revision B.04, M. J. Frisch, G. W. Trucks, H. B. Schlegel, G. E. Scuseria, M. A. Robb, J. R. Cheeseman, V. G. Zakrzewski, J. A. Montgomery, Jr., R. E. Stratmann, J. C. Burant, S. Dapprich, J. M. Millam, A. D. Daniels, K. N. Kudin, M. C. Strain, O. Farkas, J. Tomasi, V. Barone, M. Cossi, R. Cammi, B. Mennucci, C. Pomelli, C. Adamo, S. Clifford, J. Ochterski, G. A. Petersson, P. Y. Ayala, Q. Cui, K. Morokuma, D. K. Malick, A. D. Rabuck, K. Raghavachari, J. B. Foresman, J. Cioslowski, J. V. Ortiz, B. B. Stefanov, G. Liu, A. Liashenko, P. Piskorz, I. Komaromi, R. Gomperts, R. L. Martin, D. J. Fox, T. Keith, M. A. Al-Laham, C. Y. Peng, A. Nanayakkara, C. Gonzalez, M. Challacombe, P. M. W. Gill, B. G. Johnson, W. Chen, M. W. Wong, J. L. Andres, M. Head-Gordon, E. S. Replogle, J. A. Pople, Gaussian, Inc., Wallingford CT, **2004**.
- [21] V. Pophristic, S. Vemparala, I. Ivanov, Z. Liu, M. L. Klein, W. F. DeGrado, *J. Phys. Chem. B* **2006**, *110*, 3517–3526.
- [22] R. Vargas, J. Garza, D. Dixon, B. Hay, *J. Phys. Chem. A* **2001**, *105*, 774–778.
- [23] a) R. J. Doerksen, B. Chen, D. Liu, G. N. Tew, W. F. DeGrado, M. L. Klein, *Chem. Eur. J.* **2004**, *10*, 5008–5016; b) R. J. Doerksen, B. Chen, M. L. Klein, *Chem. Phys. Lett.* **2003**, *380*, 150–157.
- [24] G. R. Desiraju, *Acc. Chem. Res.* **1996**, *29*, 441–449.
- [25] a) N. Kobko, J. J. Dannenberg, *J. Phys. Chem. A* **2003**, *107*, 10389–10395; b) T. F. A. de Greef, M. M. J. Smulders, M. Wolffs, A. P. H. J. Schenning, R. P. Sijbesma, E. W. Meijer, *Chem. Rev.* **2009**, *109*, 5687–5754.
- [26] Y. Zhou, M. Xu, T. Yi, S. Xiao, Z. Zhou, F. Li, C. Huang, *Langmuir* **2007**, *23*, 202–208.
- [27] A. Tanatani, A. Yokoyama, I. Azumaya, Y. Takakura, C. Mitsui, M. Shiro, M. Uchiyama, A. Muranaka, N. Kobayashi, T. Yokozawa, *J. Am. Chem. Soc.* **2005**, *127*, 8553–8561.
- [28] P. E. Blöchl, *Phys. Rev. B* **1994**, *50*, 17953–17979.
- [29] G. Kresse, J. Joubert, *Phys. Rev. B* **1999**, *59*, 1758–1775.
- [30] H. J. Monkhorst, J. D. Pack, *Phys. Rev. B* **1976**, *13*, 5188–5192.

Received: September 24, 2009
Published online: December 18, 2009